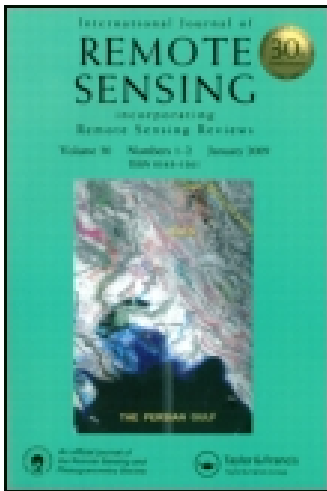


This article was downloaded by: [The University of Texas at El Paso]

On: 29 December 2014, At: 06:58

Publisher: Taylor & Francis

Informa Ltd Registered in England and Wales Registered Number: 1072954 Registered office: Mortimer House, 37-41 Mortimer Street, London W1T 3JH, UK



International Journal of Remote Sensing

Publication details, including instructions for authors and subscription information:

<http://www.tandfonline.com/loi/tres20>

Object-oriented change detection based on the Kolmogorov-Smirnov test using high-resolution multispectral imagery

Yuqi Tang^a, Liangpei Zhang^a & Xin Huang^a

^a State Key Laboratory of Information Engineering in Surveying, Mapping and Remote Sensing (LIESMARS), Wuhan University, Wuhan, China

Published online: 07 Jul 2011.

To cite this article: Yuqi Tang, Liangpei Zhang & Xin Huang (2011) Object-oriented change detection based on the Kolmogorov-Smirnov test using high-resolution multispectral imagery, *International Journal of Remote Sensing*, 32:20, 5719-5740, DOI: [10.1080/01431161.2010.507263](https://doi.org/10.1080/01431161.2010.507263)

To link to this article: <http://dx.doi.org/10.1080/01431161.2010.507263>

PLEASE SCROLL DOWN FOR ARTICLE

Taylor & Francis makes every effort to ensure the accuracy of all the information (the "Content") contained in the publications on our platform. However, Taylor & Francis, our agents, and our licensors make no representations or warranties whatsoever as to the accuracy, completeness, or suitability for any purpose of the Content. Any opinions and views expressed in this publication are the opinions and views of the authors, and are not the views of or endorsed by Taylor & Francis. The accuracy of the Content should not be relied upon and should be independently verified with primary sources of information. Taylor and Francis shall not be liable for any losses, actions, claims, proceedings, demands, costs, expenses, damages, and other liabilities whatsoever or howsoever caused arising directly or indirectly in connection with, in relation to or arising out of the use of the Content.

This article may be used for research, teaching, and private study purposes. Any substantial or systematic reproduction, redistribution, reselling, loan, sub-licensing, systematic supply, or distribution in any form to anyone is expressly forbidden. Terms &

Conditions of access and use can be found at <http://www.tandfonline.com/page/terms-and-conditions>

Object-oriented change detection based on the Kolmogorov–Smirnov test using high-resolution multispectral imagery

YUQI TANG, LIANGPEI ZHANG and XIN HUANG*

State Key Laboratory of Information Engineering in Surveying, Mapping and Remote Sensing (LIESMARS), Wuhan University, Wuhan, China

(Received 4 February 2010; in final form 1 June 2010)

In this article, we propose a novel method of object-oriented change detection for high-resolution remote-sensing imagery. The method consists of three main parts: image segmentation, object adjusting and change detection. We use the Fractal Net Evolution Approach to segment the multi-temporal images. Then we adjust the object maps. By merging the objects in relatively large areas, the object-adjusting algorithm aims to obtain a set of objects with different sizes, which coincide better with the real ground objects than the single-scale results. In the third part, the Kolmogorov–Smirnov two-sample test detects each pair of objects in the multi-temporal object maps with multi-scale. The calculated value of the D -statistic is compared to the threshold of a user-defined significance level. Through these three processes, we can make full use of the spatial and spectral features in high-resolution images to detect changes. According to our experiments in two study areas employing QuickBird imagery, the overall errors of our method decreased by more than 1000 pixels compared with the conventional object-oriented change vector analysis. The proposed method can also avoid the errors resulting from classification in the method of post-classification comparison.

1. Introduction

Change is defined as ‘the result of something becoming different’. Both natural and artificial changes can take place. Natural changes usually occur periodically, such as the phenological change of deciduous plants. However, artificial changes are often irreversible. These result from human activities. Change detection is ‘the process of identifying differences in the state of an object or phenomenon by observing it at different times’ (Singh 1989). Detection of natural changes can help us to know about the growth situation of vegetation, whereas anthropogenic change detection is important for natural-resources management and urban-development monitoring (Olson *et al.* 2004). Change-detection analysis is one of the most important applications in remote-sensing image processing. The most popular methods are change vector analysis (CVA) and post-classification comparison.

However, with the development of high spatial resolution remote-sensing satellites, the amount of image information has increased dramatically. This information presents the details of ground objects in the visual field. Until now, change detection

*Corresponding author. Email: huang_w hu@163.com

using high-resolution imagery has not been carried out as well as it has been for low- and middle-resolution imagery. The improved spatial resolution has not brought about superior detection capability, as the autocorrelation is no longer easy to approximate by a pulse function in high-resolution imagery. With high spatial resolution, the pixels are not spatially independent, resulting in the conventional change-detection techniques becoming ineffective (Bovolo 2009).

There have been some techniques that conform to the increase in spatial resolution. Some of them have achieved the incorporation of various image features besides the spectral feature. Huang *et al.* (2007) proposed a method of spatial feature extraction for the classification of high-resolution multispectral imagery. It is an extension of the pixel shape index (PSI) (Zhang *et al.* 2006). In addition, use can be made of morphological texture features (Huang *et al.* 2009). However, this was primarily aimed at the classification of high-resolution imagery rather than change detection.

Besides the extraction of various features, the images can be processed in other ways. The object-oriented technique is one of the most typical methods. It has been proved to be suitable for high-resolution imagery. The principle of the object-oriented technique is the processing of a set of pixels as a unit, which is called an object. These pixels of the same object are adjacent in space and spectrally similar to each other. Thus one can process them as a homogeneous entity. In this way, full use can be made of the various kinds of information contained in the images, such as spatial and spectral information. In addition, processing an object as a unit can remove redundant details resulting from the increase in spatial resolution. These characteristics all perfectly meet the needs of processing high-resolution imagery. In other words, the object-oriented technique can reduce the local spectral variation and suppress the salt-pepper effect in high-resolution imagery. The first commercial software for object-oriented image analysis was eCognition (Definiens, Munchen, Germany). Bruzzone and Prieto (2000) applied it to change detection in 2000, which effectively improved the change-detection result of high-resolution imagery. But it was only utilized at a single scale, which could not conform to the various sizes of ground objects in reality. Walter (2003) introduced the object-oriented technique to post-classification comparison. It still did not settle the problem of single scale. In addition, the object-oriented post-classification comparison brought about attached errors that resulted from the classification. Bovolo (2009) applied an object-oriented technique with multi-scale to CVA. It resolved the shortcomings of single scale and classification error, but it did not dispose of the limitations of CVA. The dominant limitation of CVA is its too heavy reliance on the spectral features. It only considers the spectral values of pixels to construct the change vectors. In particular, the pixel values used in this method to build the change vectors were the mean values of pixels in every object. These deviate greatly from the real ones, which could result in considerable errors.

This article introduces a novel method of object-oriented change detection using high-resolution imagery. As multi-temporal images are taken with time differences of several years and in different seasonal and lighting conditions, registration and radiometric correction must be performed as pre-processes. In addition, according to the objectives of detecting the anthropogenic changes in the observed field, the masking of vegetation and shadow is necessary. Moreover, median filtering is necessary to remove the redundant details in the high-resolution images. After the segmentation of multi-temporal images using the Fractal Net Evolution Approach (FNEA) (Batz and Schape 2000), adjustments are made to the object maps. If some objects express different parts of the same ground object, these are merged to be an object

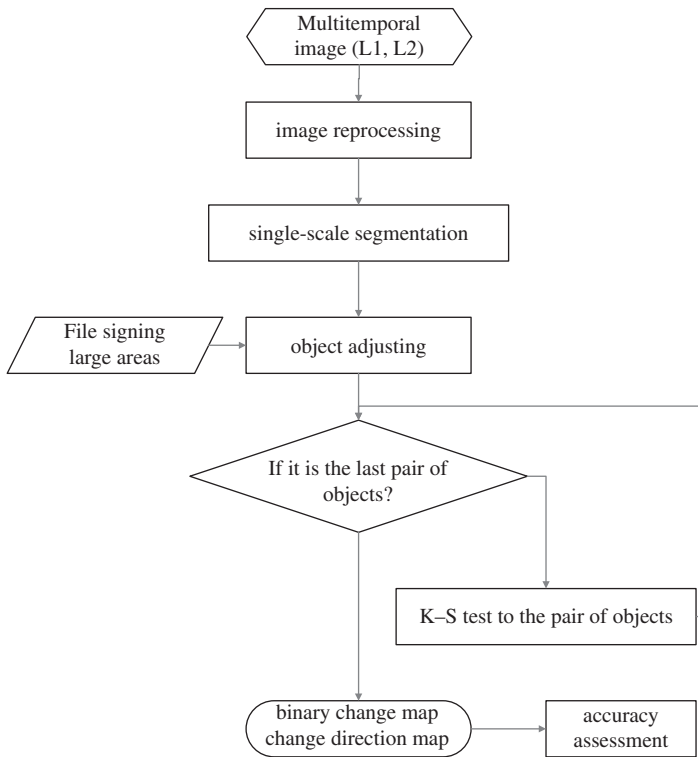


Figure 1. Process flow.

whose scale would become larger. By this means, multi-scale segmentation results are acquired. Then every pair of objects in the multi-temporal images are tested with the Kolmogorov–Smirnov (K–S) test, which is a non-parametric statistical test. It can be used to determine if two sets of samples differ significantly (Siegel and Castellan 1988). During this process, the maximum absolute difference of statistical probabilities for each pair of objects is calculated, considering the spectral value of every pixel in the initial images. In this way, full use can be made of the useful spectral information in the initial images. Compared to the pixel-based CVA (Johnson and Kasischke 1998) and the object-oriented CVA (Bovolo 2009), the proposed method can make full use of information in the multi-temporal images while effectively avoiding the errors brought from the spectral mean values of every object. The processing flow of the proposed method is shown in figure 1.

2. Methodology

2.1 Segmentation using the Fractal Net Evolution Approach

In the proposed method, the FNEA is employed to segment the high-resolution images. It adopts the individual pixel value and its neighbourhood to compute the colour criterion (h_{colour}) and the shape or spatial criterion (h_{shape}). According to these, the image can be segmented into an object map by the heterogeneity (S_f) of every pair of neighbouring objects. This heterogeneity is a weighed sum of the colour criterion

and the shape or spatial criterion (equation (1)). Each of the objects in the resulting map includes the relatively homogeneous pixels neighbouring each other:

$$S_f = \omega_{\text{colour}} h_{\text{colour}} + (1 - \omega_{\text{colour}}) h_{\text{shape}}, \quad (1)$$

where $0 \leq \omega_{\text{colour}} \leq 1$ is the user-defined weight of spectrum. It is relative to the weight of shape. If the spectral feature is to be emphasized, the value of ω_{colour} should be larger. Conversely, when the spatial feature is more important, the value of $(1 - \omega_{\text{colour}})$, which is the weight of shape or space, should be larger.

In equation (1), the colour criterion (h_{colour}) is a weighted mean of the change in standard deviation of the k th band of the image:

$$h_{\text{colour}} = \sum_{k=1}^m \omega_k [n_{\text{mg}} \sigma_k^{\text{mg}} - (n_{\text{ob1}} \sigma_k^{\text{ob1}} + n_{\text{ob2}} \sigma_k^{\text{ob2}})], \quad (2)$$

where ω_k is the weight of the k th band, n_{mg} is the number of pixels in the object after merging, σ_k^{mg} is the standard deviation of spectral values in the object after merging, n_{ob1} and n_{ob2} are the numbers of pixels in the objects before merging, and σ_k^{ob1} and σ_k^{ob2} are the standard deviations of spectral values in the objects before merging.

On the other hand, the shape or spatial criterion (h_{shape}) is a weighted sum of two parts, which are compactness and smoothness:

$$h_{\text{shape}} = \omega_{\text{cpt}} h_{\text{cpt}} + (1 - \omega_{\text{cpt}}) h_{\text{smooth}}, \quad (3)$$

where $0 \leq \omega_{\text{cpt}} \leq 1$ is the user-defined weight of compactness. This equation estimates the value of the shape criterion through every merge by calculating the weighted sum of the compactness and smoothness criteria. Equations (4) and (5) show the formulae for the compactness and smoothness criteria separately:

$$h_{\text{cpt}} = n_{\text{mg}} \frac{l_{\text{mg}}}{\sqrt{n_{\text{mg}}}} - \left(n_{\text{ob1}} \frac{l_{\text{ob1}}}{\sqrt{n_{\text{ob1}}}} + n_{\text{ob2}} \frac{l_{\text{ob2}}}{\sqrt{n_{\text{ob2}}}} \right), \quad (4)$$

$$h_{\text{smooth}} = n_{\text{mg}} \frac{l_{\text{mg}}}{b_{\text{mg}}} - \left(n_{\text{ob1}} \frac{l_{\text{ob1}}}{b_{\text{ob1}}} + n_{\text{ob2}} \frac{l_{\text{ob2}}}{b_{\text{ob2}}} \right), \quad (5)$$

where l_{mg} is the pixel perimeter length of the object after merging; l_{ob1} and l_{ob2} are the pixel perimeter lengths of the objects before merging; b_{mg} is the pixel perimeter length of the minimum enclosing rectangle of the object after merging; and b_{ob1} and b_{ob2} are the pixel perimeter lengths of the minimum enclosing rectangle of the objects before merging.

At the beginning of segmentation, every pixel was regarded as an individual object. After calculating the heterogeneity (S_f) of every pair of neighbouring objects, these are compared to the user-defined value of scale, which can be regarded as the threshold of heterogeneity. If the value of S_f is lower than the scale, this pair of objects is merged; otherwise, they are preserved as two individual objects. These procedures are repeated until no pair of objects remains that could be merged. Then the object map can finally be obtained. From the above, the selection of scale, the weights of spectrum and compactness are critical to the segmentation result, especially to the scale, as they decide

the size of objects in the object map. In most current research, the scale selection is still an empirical process.

2.2 The Kolmogorov–Smirnov test

The K–S test was proposed by Smirnov (1948). It is a goodness-of-fit test for any statistical distribution and is a form of minimum distance estimation. It is used as a non-parametric test of equality of one-dimensional probability distributions to compare a sample with a reference probability distribution (K–S one-sample test) or to compare two samples (K–S two-sample test) (Wikipedia 2009). In our method, we want to detect the changes between any pair of multi-temporal images. Therefore, the K–S two-sample test will be introduced in the following text.

If two sets of pixels in the pair of multi-temporal images are signed as L1 and L2, their cumulative frequencies can be obtained by the following equations:

$$S_1(X) = \frac{K_1}{n_1}, \quad (6)$$

$$S_2(X) = \frac{K_2}{n_2}, \quad (7)$$

where n_1 and n_2 are the total number of pixels in L1 and L2, X is a certain spectral value, K_1 and K_2 are the numbers of pixels with spectral values less than X in L1 and L2.

By adjusting the value of X , the maximum absolute difference between the two cumulative frequencies can be calculated, which is called the D -statistic:

$$D_{1,2} = \max |S_1(X) - S_2(X)|. \quad (8)$$

In order to judge whether the two sets of samples are different, a level of significance is chosen according to the experimental requirement. This can determine the threshold value of difference. When $n_1 = n_2$ and they are both <25 , there are three levels that could be chosen: 0.10, 0.05 and 0.01 (Pearson and Hartley 1972). When either n_1 or n_2 is >25 , there are different formulae for the threshold in each of six significance levels: 0.10, 0.05, 0.025, 0.01, 0.005 and 0.001 (Smirnov 1948). With different values of n_1 and n_2 , there are various thresholds for a certain level. If the D -statistic ($D_{1,2}$) is less than the threshold, it can be concluded that there is no difference between the two sets of samples.

2.3 Object-oriented change detection based on the Kolmogorov–Smirnov test

In the proposed method, the K–S two-sample test is applied to object-oriented change detection. The changes detected are the anthropogenic changes.

After pre-processing of registration, radiometric correction, masking of vegetation and shadow and median filtering, the FNEA is used to segment the pair of multi-temporal images simultaneously with the same parameters. These parameters include the value of scale, the weight of spectrum and compactness. In this way, it can be ensured that the two sets of objects in the pair of segmented images have the same numbers, and each pair of objects also have the same pixels.

The next step adjusts the object maps. By investigating every object in the object maps, the objects constituting a same ground object are merged. In this way, a pair of segmentation results can be obtained with multi-scale objects. In other words, the sizes of objects in each of the segmented maps are levelled. The large ground objects are segmented into objects with a large size, while the small ground objects correspond to small-sized objects.

Changes are then detected by applying the K–S two-sample test to the multi-scale object maps. The processing unit in this step is every pair of objects in the pair of multi-temporal images. As there are two same sets of pixels in each pair of objects, equations (6) and (7) can be modified as follows:

$$S_1(X) = \frac{K_1}{n}, \quad (9)$$

$$S_2(X) = \frac{K_2}{n}. \quad (10)$$

where n is the number of pixels in each of the pair of objects.

After calculating the two cumulative probabilities shown in equations (9) and (10), the value of the D -statistic is computed by equation (8). By choosing an appropriate significance level, it is possible to judge whether the D -statistic is less than the threshold corresponding to the level. If it is not less than the threshold, the conclusion is that the region covered by this pair of objects has changed. These procedures are repeated object by object until every pair of objects has been detected. Then the binary change map is obtained.

According to the binary change map so obtained, the change direction maps can be formed as follows. The changed areas are separated into two parts. The first part contains the changed areas with increasing spectral reflectivity, while the other part contains the changed areas with decreasing spectral reflectivity. As the spectral reflectivity of every kind of ground object concentrates in a certain range of the spectral band, the class of ground objects can be deduced according to the band with the largest change.

3. Experiment

3.1 Study area

In the experiment, a pair of multi-temporal high-resolution images acquired by the QuickBird satellite in 2002 and 2005, was employed. They cover approximately the same area of Wuhan in central China. In order to preserve the spectral information as much as possible, the multispectral images were used in the experiments. Each has four spectral bands: the red band (0.45–0.52 μm), the green band (0.52–0.60 μm), the blue band (0.63–0.69 μm) and the near infrared band (0.76–0.90 μm).

Two study areas (site 1 and site 2) in this pair of multi-temporal high-resolution images were selected, and the experiments were performed separately. Site 1 was around the campus of Wuhan University (figure 2(a) and (b)), and site 2 was the northern part of Wuchang (figure 2(c) and (d)) in Wuhan City. Each study area covered an area of 400 pixels \times 400 pixels, with a spatial resolution of 2.4 m. The ground objects of site 1 were roofs, vegetation (grass and trees), water (swimming pools and ponds), bare land, rubber ground (playgrounds), roads and shadows. Compared

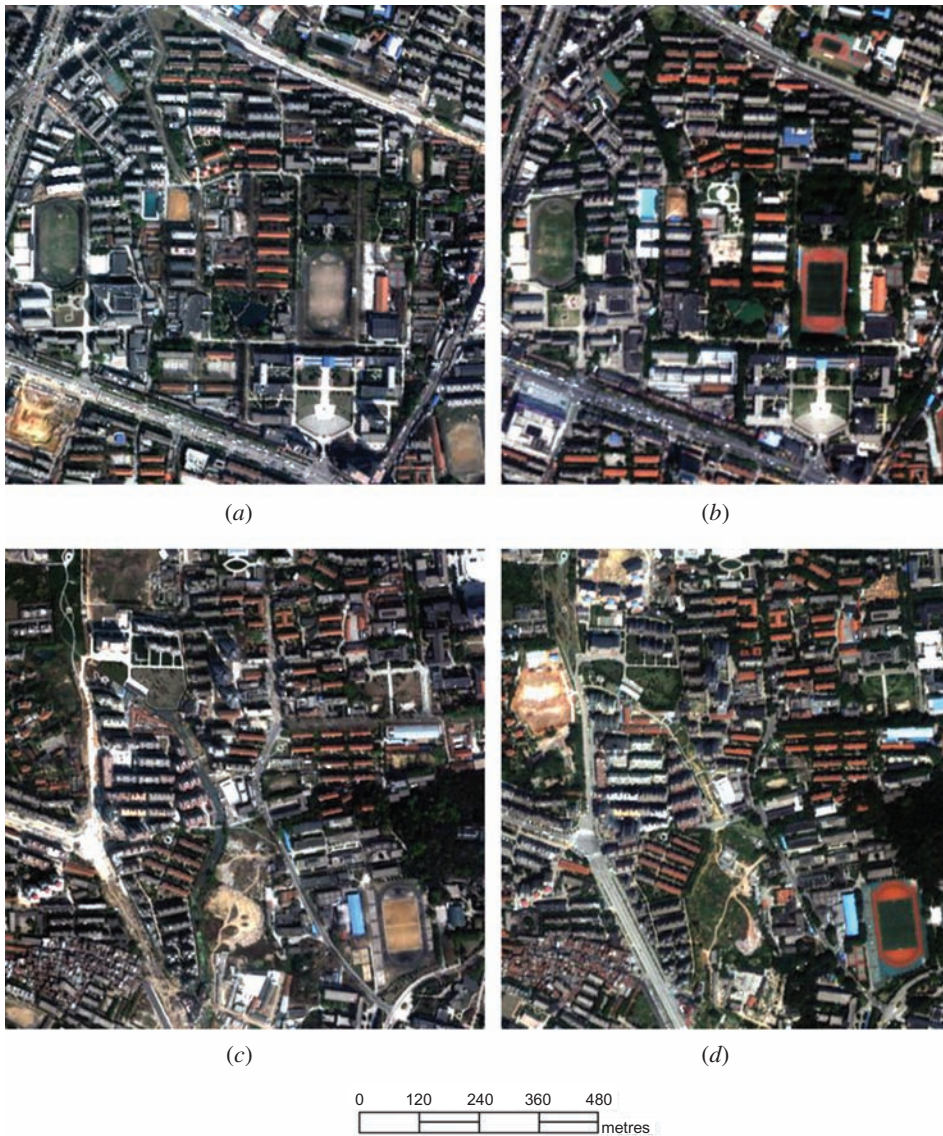


Figure 2. Study area of (a) site 1 in 2002, (b) site 1 in 2005, (c) site 2 in 2002 and (d) site 2 in 2005.

to site 1, site 2 is short of the water category. The changes to be detected are the anthropogenic changes that can reflect city development, such as the appearance or disappearance of man-made green areas and the construction or reconstruction of buildings.

A good pre-processing can remove some valueless difference information in the multi-temporal images and improve the result of change detection. In the experiment, the 2002 image was taken as the reference one and the 2005 image was processed based on it. First, registration was performed using the software of Envi 4.6 (ITT, New York, USA). Eight ground-control points (GCPs) were used separately in site 1 and site 2,

both employing the polynomial method with one degree and using the resampling method of near neighbour. As they were recorded on different dates of the year and also at different times of the day, the two images were acquired in considerably different illumination conditions. Therefore, a relative radiometric correction to the image of 2005 was performed on the basis of the one of 2002. By selecting eight fake invariable points (PIFs) separately on each site, a linear regression was carried out on every spectral band. The aim was to detect the anthropogenic changes reflecting the development of this area; therefore, the changes resulting from vegetation growth and shadow covering would affect this work. Therefore, the areas covered by vegetation or shadow were masked in both images for each study site. Lastly, a median filter was applied to each image to reduce the redundant details.

3.2 Experiment of site 1

3.2.1 Statistical evaluation. In order to evaluate the proposed method soundly, the analysis of the experimental results of site 1 contains several perspectives as follows.

In the segmentation procedure, different spatial scales would result in different object maps; consequently, the results of change detection would vary. Before evaluating the statistical results with various scales, it is worth noting that the results must be analysed with small scales separately from the ones with large scales. That is because when the number of pixels in a certain object is <25 , the threshold of a certain significance level is different from when >25 . As detected by different thresholds, the results with various scales cannot be compared. Therefore, using scales ranging from 6 to 22 to choose the optimal one, in the experiments of site 1, our results were divided into two parts: the results with scales less than eight and the results with scales larger than eight.

The result of change detection can be evaluated by the numbers of false alarms and missed alarms (table 1), and their sum, which is called the overall error (figure 3). It can be seen that the numbers of overall errors ranged from 9800 to 11 500 pixels, while the ranges of false alarms and missed alarms were relatively larger. Combining table 1 with figure 3, the following can be deduced:

1. In the results with scales not larger than eight, every object has a different number of pixels, some of which are larger than 25, while others are not. Their thresholds at a specific significance level are different. Thereby, it is hard to summarize any rule for this part of the results.
2. In the results with relatively small scales larger than eight, the size of objects was small. There were a large number of missed alarms, which primarily occurred in the relatively similar parts of the large changed area. This was because that changed area contained many objects, some of whose variations were less than others. Thereby, it was possible to detect these objects with relatively smaller variations as unchanged objects, which would cause some missed alarms. On the other hand, the number of false alarms in this condition would be less.
3. In addition, in the results with relatively large scales (larger than eight), the size of objects was large. There were a large number of false alarms caused by the changed objects covering the edge of changed areas. These objects likely contained some unchanged areas near the changed ones. Nevertheless, the missed alarms would be less in that situation.

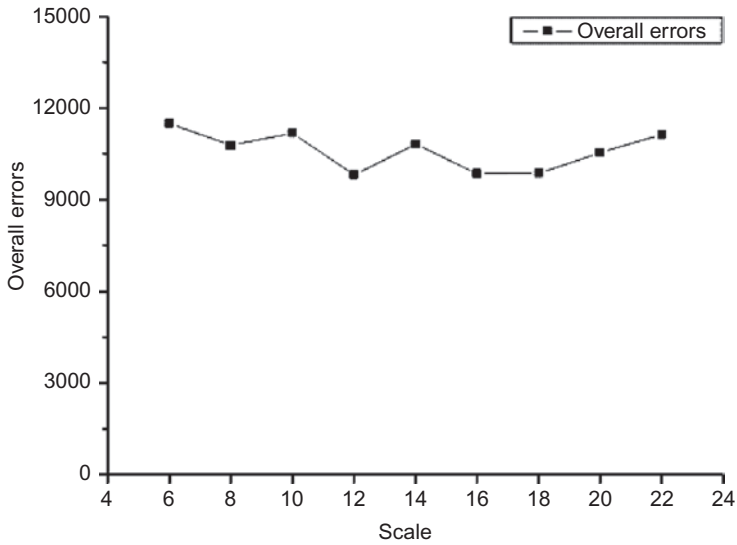


Figure 3. The overall errors of our method in site 1.

Table 1. The false alarms and missed alarms of our method in site 1.

Scale	Significance level	False alarms	Missed alarms
6	0.01	6375	5120
8	0.01	5107	5669
10	0.01	4174	6999
12	0.01	5615	4201
14	0.01	5748	5069
16	0.01	6165	3689
18	0.01	6529	3331
20	0.01	6857	3677
22	0.01	8184	2942

Additionally, there were also other kinds of false alarms due to illumination difference or shadow covering. On the basis of the above, an appropriate scale could result in reasonable object maps and a reduction of the number of false alarms and missed alarms to as few as possible. According to the results in figure 3, it can be concluded that the optimal scale of our experiment for site 1 was about 12.

With a certain scale, different significance levels mean different thresholds during change detection based on the K-S test. These thresholds could determine whether there are changes in the area covered by the object. Choosing the optimal level is also an empirical process. The optimal level varies with different scales (table 2). In site 1, the optimal level of significance with the scale 12 was at the level of 0.01. However, when the scale was 16, the optimal level would change to the 0.005 level.

To demonstrate the validity of object adjusting in our experiments, the results with multi-scale were compared to the results with a single scale. The difference between their overall errors is shown in figure 4. It was found that there was a dramatic

Table 2. The optimal significance level varies with different scales in site 1.

Scale	Significance level	Overall error
12	0.001	9877
12	0.005	10 943
12	0.01	9816
12	0.025	9956
12	0.05	9948
12	0.1	10 202
16	0.001	10 145
16	0.005	9719
16	0.01	9854
16	0.025	10 538
16	0.05	9880
16	0.1	10 422

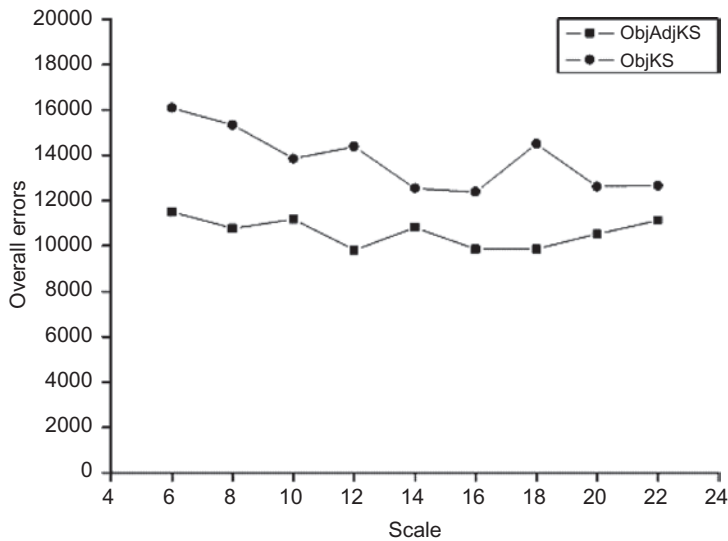


Figure 4. The overall errors of our method with and without object adjusting in site 1.

improvement by adding the object-adjusting step. In other words, the change detection error of the proposed method was obviously less than the error without object adjusting.

To confirm the effectiveness of object-oriented techniques in the processing of high-resolution remote-sensing imagery, the results were compared to the pixel-based CVA (Johnson and Kasischke 1998) with an empirical optimal threshold of nine. With the overall errors numbering 12 295 pixels, the pixel-based CVA was more than 2450 pixels greater than our method. In addition, in order to prove the superiority of the proposed method in relative object-oriented change-detection research, the overall errors of our method were compared to the object-oriented CVA (Bovolo 2009) (figure 5). Table 3 shows their differences of false alarms and missed alarms. It can be seen that, with any scale in the selected range, the overall error of our method was less than the ones of

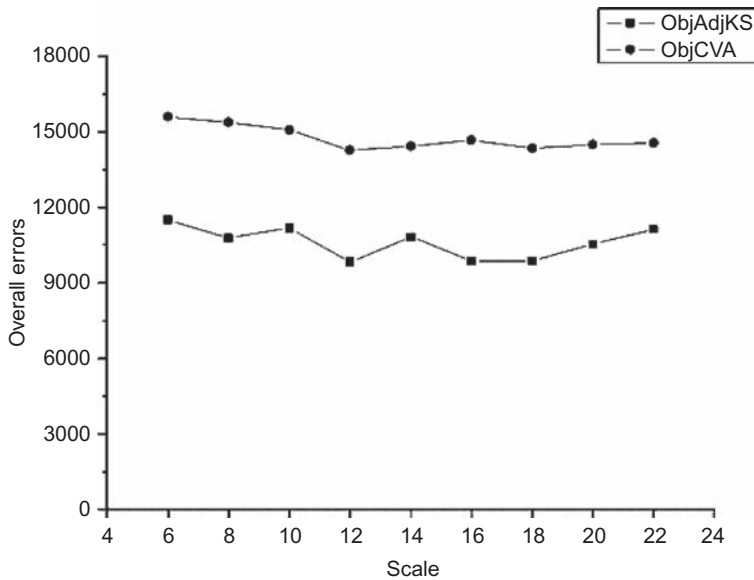


Figure 5. The overall errors of our method and the object-oriented CVA in site 1.

Table 3. The false alarms and missed alarms of our method and object-oriented CVA in site 1.

Scale	ObjCVA -false alarms	ObjAdjKS-false alarms	ObjCVA -missed alarms	ObjAdjKS-missed alarms
6	7999	6375	7596	5120
8	7693	5107	7687	5669
10	7661	4174	7412	6999
12	6870	5615	7398	4201
14	6811	5748	7608	5069
16	6619	6165	8058	3689
18	6283	6529	8066	3331
20	6222	6857	8271	3677
22	6115	8184	8438	2942

the object-oriented CVA for over 3000 pixels in the experiments of site 1. In this analysis, the significance level of 0.01 was chosen for the proposed method. The empirical optimal threshold of the object-oriented CVA was two.

3.2.2 Visual inspection. According to our experiments with site 1, the optimal result had scale 12 and level 0.01. The binary change map is shown in figure 6(a), in which objects in white present the regions that have changed, and objects in black indicate the unchanged areas. The change direction maps are shown in figures 6(b) and (c). Due to the bands' range of the multispectral QuickBird images, in the change direction maps of site 1, the areas with grey levels of 255 and 195 mainly represent the changes in man-made buildings, such as roofs and roads. The grey level of 135 primarily means changed areas of bare land or rubber ground, while the value of 65 shows the changed regions covered by vegetation. It is worth noting that in these changed regions covered by vegetation, the changes represent ones from other kinds

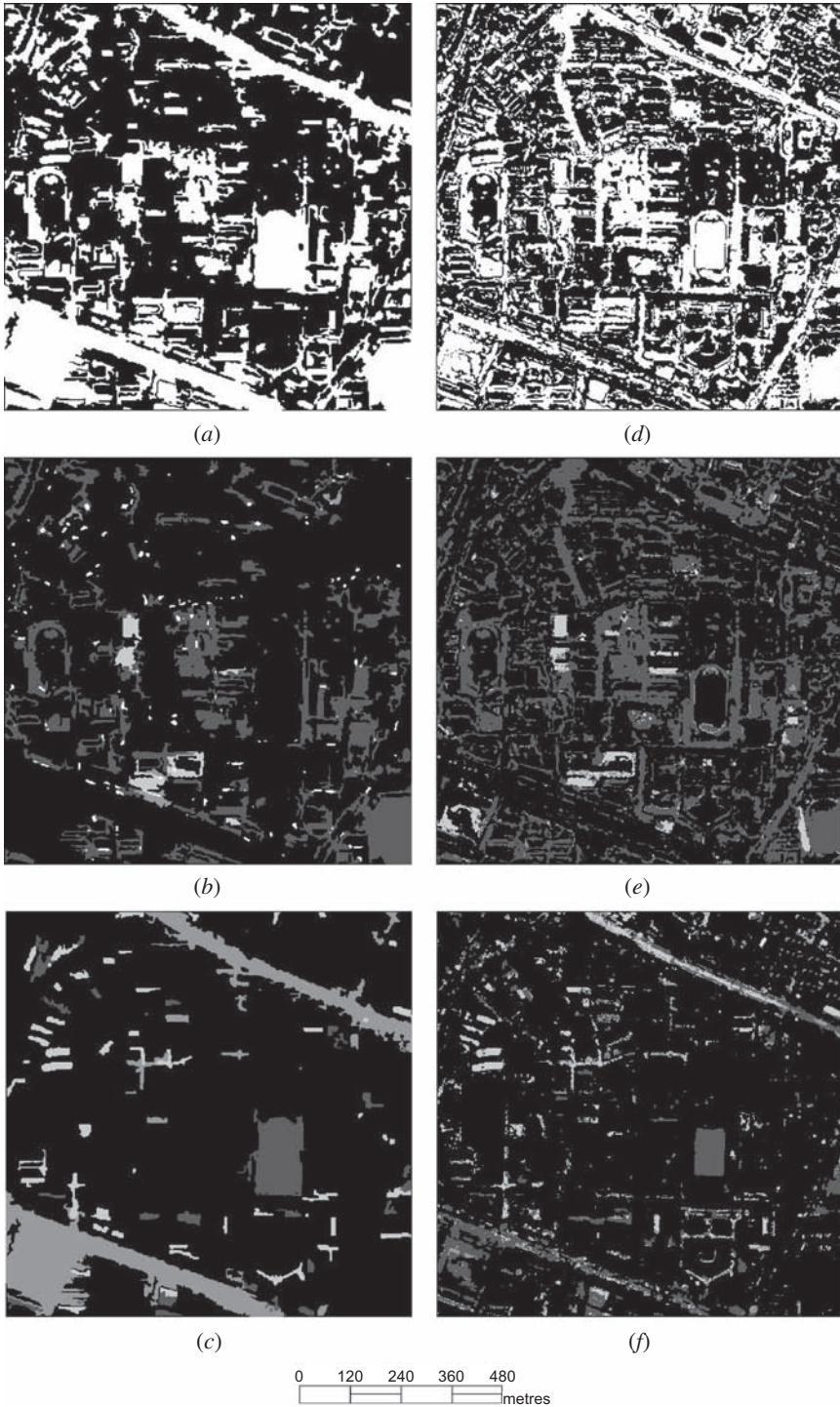


Figure 6. Comparison of the results of our method and the pixel-based CVA in site 1. (a) Binary change map of our method, (b) the first band of change direction map of our method, (c) the second band of change direction map of our method, (d) binary change map of the pixel-based CVA, (e) the first band of change direction map of the pixel-based CVA and (f) the second band of change direction map of the pixel-based CVA.

to vegetation and also the changes from vegetation to other kinds, but not the changes reflecting vegetation growth. Figure 6(d)–(f) shows the best results of the pixel-based CVA. The salt-pepper effect was serious in the result of pixel-based CVA, while the local spectral variation was effectively depressed by the proposed method. This proved the superiority of the object-oriented techniques in the processing of high-resolution remote-sensing imagery. Additionally, it is useful to compare the optimal result of the proposed method with the best results of the object-oriented CVA with a scale of 12 and a threshold of two (figure 7(d)–(f)). The integrity of the proposed method in the large areas is obviously better than the object-oriented CVA.

When compared, it was seen that the binary change map of the proposed method was approximately the same as the reference one (figure 8). However, there were some inevitable errors. The false alarms were mainly due to the relatively larger objects on the edges of the changed areas rather than the real ones. On the other hand, the missed alarms result primarily from the relatively small objects in the changed areas. As the size of objects was less than the area that really changed, some of these pairs of objects were more similar than other pairs. Therefore, it was likely that these similar objects were detected as unchanged.

3.3 Experiment on site 2

3.3.1 Statistical evaluation. Similarly to the site 1, we analysed our experimental results of site 2 by the following perspectives.

In the segmentation procedure, the results with small scales were analysed separately from the ones with large scales. Using scales ranging from 4 to 26 to choose the optimal one, in our experiments of site 2, our results were divided into two parts: the results with scales not larger than eight and the results with scales larger than eight. The results of false alarms and missed alarms are shown in table 4, while the overall errors are shown in figure 9. It is seen that the numbers of overall errors for site 2 ranged from 5000 to 6450 pixels. Combining table 4 with figure 9, the following conclusions can be reached:

1. In the results with scales not larger than eight, it is hard to summarize any rule.
2. In the results with relatively small scales larger than eight, there were a large number of missed alarms, which primarily occurred in the relatively similar parts in the large changed area. The false alarms were fewer.
3. In the results with relatively large scales larger than eight, there were a large number of false alarms caused by the changed objects covering the edge of changed areas, while the probability of missing changed area would be less.

There were also other kinds of false alarms due to the illumination differences or shadow covering. Overall, an appropriate scale could restrict the numbers of false alarms and missed alarms to as few as possible, as well as the number of overall errors. According to the results in figure 9, it was concluded that the optimal scale of our experiment for site 2 was about ten.

Similarly, with a certain scale, different significance levels mean different thresholds during change detection based on the K–S test. Choosing the optimal level is an empirical process and varies with different scales. According to our experiments, the optimal level of significance for site 2 with the scale ten was the level of 0.01.

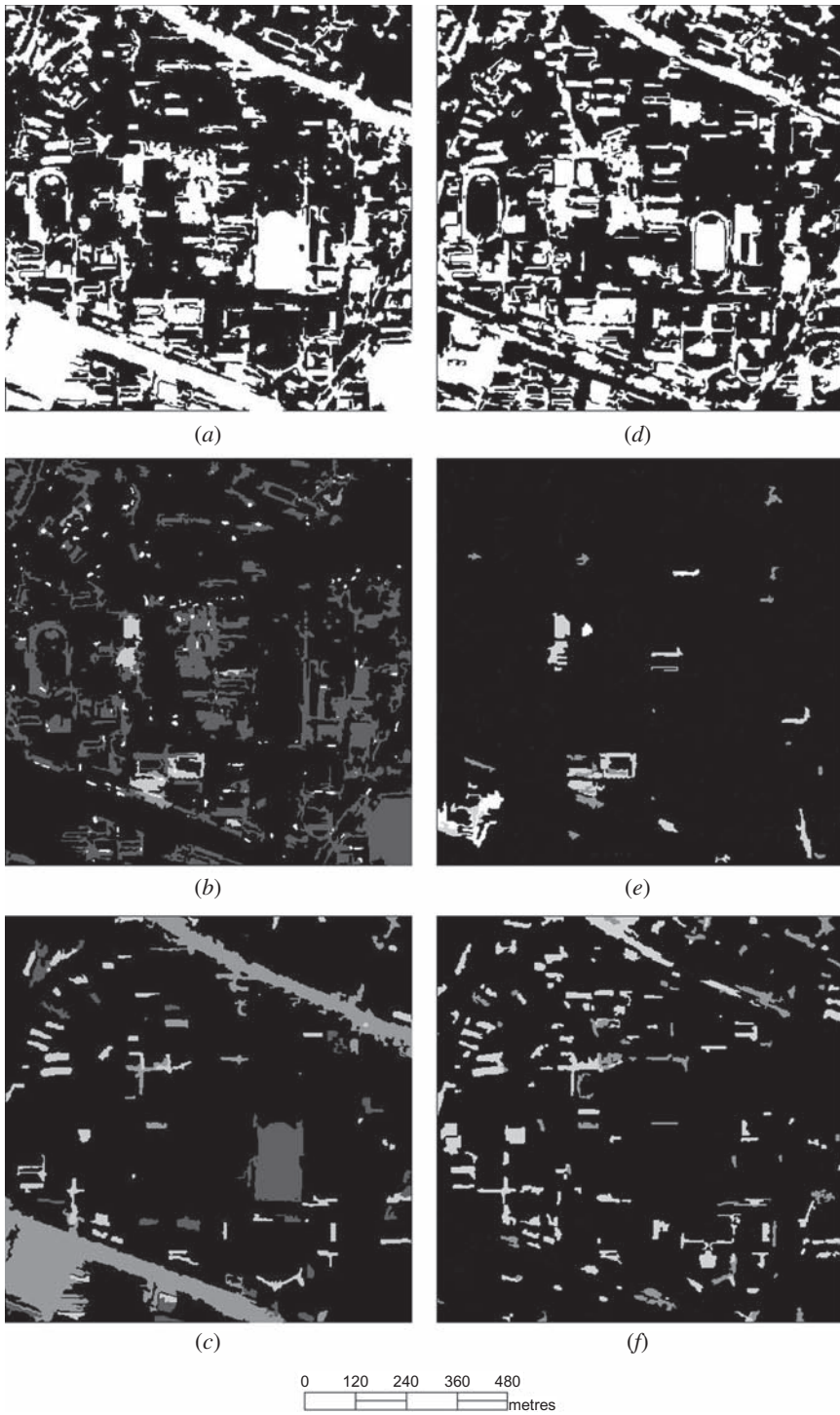


Figure 7. Comparison of the results of our method and the object-oriented CVA in site 1. (a) Binary change map of our method, (b) the first band of change direction map of our method, (c) the second band of change direction map of our method, (d) binary change map of the object-oriented CVA, (e) the first band of change direction map of the object-oriented CVA and (f) the second band of change direction map of the object-oriented CVA.



Figure 8. Reference map of changed area in site 1.

Table 4. The false alarms and missed alarms of our method in site 2.

Scale	ObjCVA-false alarms	ObjAdjKS-false alarms	ObjCVA-missed alarms	ObjAdjKS-missed alarms
4	5091	4482	2319	1954
6	5071	2188	2501	4197
8	4974	1238	2402	4440
10	4902	1518	2411	3510
12	4830	1857	2351	3353
14	4978	2457	2608	3258
16	4916	2678	2557	3018
18	4612	2759	2812	2724
20	4599	2655	2708	2657
22	4430	2862	2978	2397
24	4285	2957	3402	2153
26	4247	3197	3336	2325

To demonstrate the improvement of object adjusting in our experiments on site 2, the results with multi-scale were compared to the results with a single scale. The difference between their overall errors is shown in figure 10. It was found that there was a dramatic improvement by adding the object-adjusting step. In other words, the change detection error of our method was obviously less than the error without object adjusting.

To confirm the dominance of object-oriented techniques in the processing of high-resolution remote-sensing imagery, our results were also compared to the pixel-based CVA (Johnson and Kasischke 1998) with an empirical optimal threshold of one.

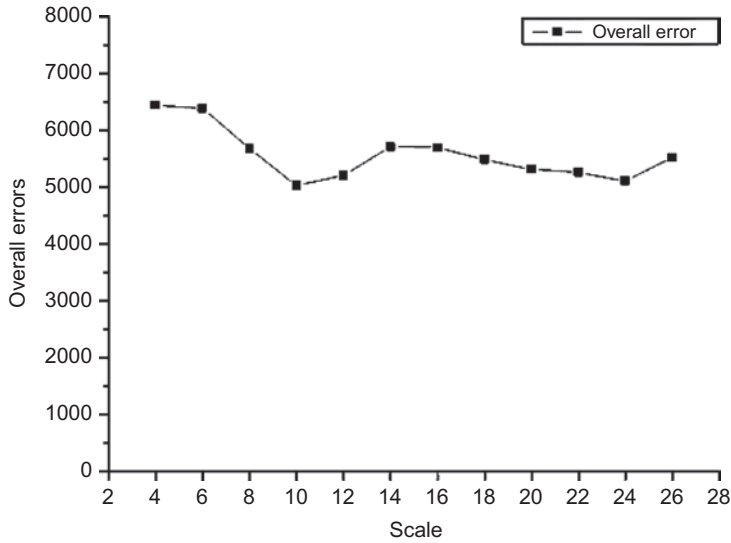


Figure 9. The overall errors of our method in site 2.

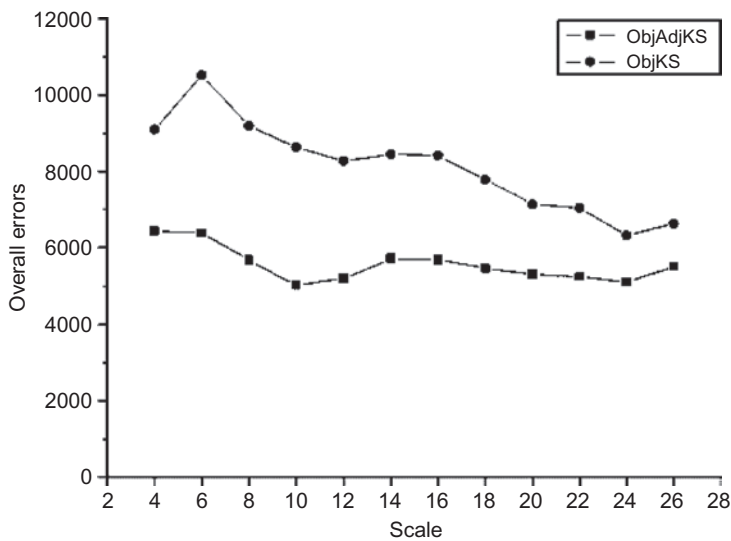


Figure 10. The overall errors of our method with and without object adjusting in site 2.

With the overall error of 21 859 pixels, the pixel-based CVA increased its number by more than 16 800 pixels from our method. It was dramatically larger than in site 1. Additionally, the overall errors of our method were compared to the object-oriented CVA (Bovolo 2009) (figure 11). Table 5 shows the differences of false alarms and missed alarms. It is seen that, with any scale in the selected range for site 2, the overall errors of our method were more than the ones of object-oriented CVA by more than 1000 pixels. In this analysis, the significance level of 0.01 was chosen for the proposed method. The empirical optimal threshold of the object-oriented CVA was one.

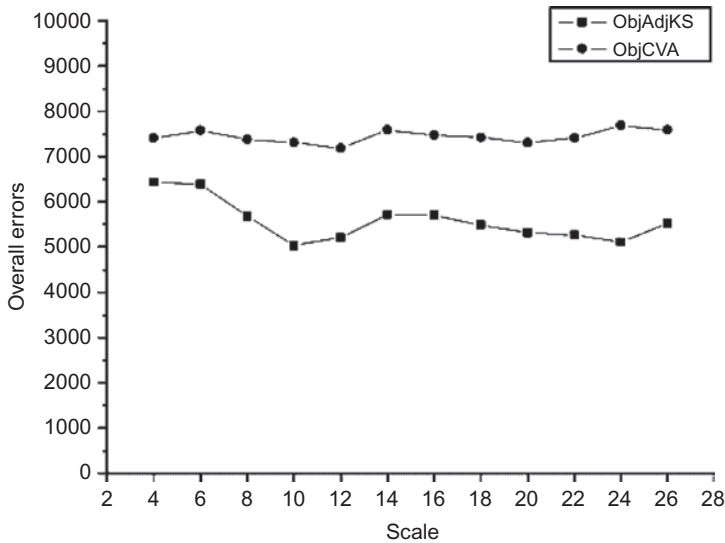


Figure 11. The overall errors of our method and the object-oriented CVA in site 2.

Table 5. The false alarms and missed alarms of our method and object-oriented CVA in site 2.

Scale	Significance level	False alarms	Missed alarms
4	0.01	4482	1954
6	0.01	2188	4197
8	0.01	1238	4440
10	0.01	1518	3510
12	0.01	1857	3353
14	0.01	2457	3258
16	0.01	2678	3018
18	0.01	2759	2724
20	0.01	2655	2657
22	0.01	2862	2397
24	0.01	2957	2153
26	0.001	3197	2325

3.3.2 Visual inspection. The best result for site 2 with a scale of 10 and level 0.01 is shown in figure 12(a). The change-direction maps are shown in figure 12(b) and (c). Similar to site 1, the areas with grey levels of 255 and 195 in the change direction maps mainly represent the changes of man-made buildings; the grey level of 135 primarily means changed areas of bare land or rubber ground; the one of 65 shows the change in areas of vegetation. The changes detected in vegetation are again the changes from other kinds to vegetation or from vegetation to other kinds, but not the changes reflecting vegetation growth. Figure 12(d)–(f) shows the best results of the pixel-based CVA. The salt-pepper effect was again serious in the result of pixel-based CVA, while the local spectral variation was effectively depressed by the proposed method. It proved the superiority of the object-oriented techniques in the processing of high-resolution remote-sensing imagery. In addition, the optimal result of the proposed method can be visually compared with the best results of the object-oriented CVA with a scale of

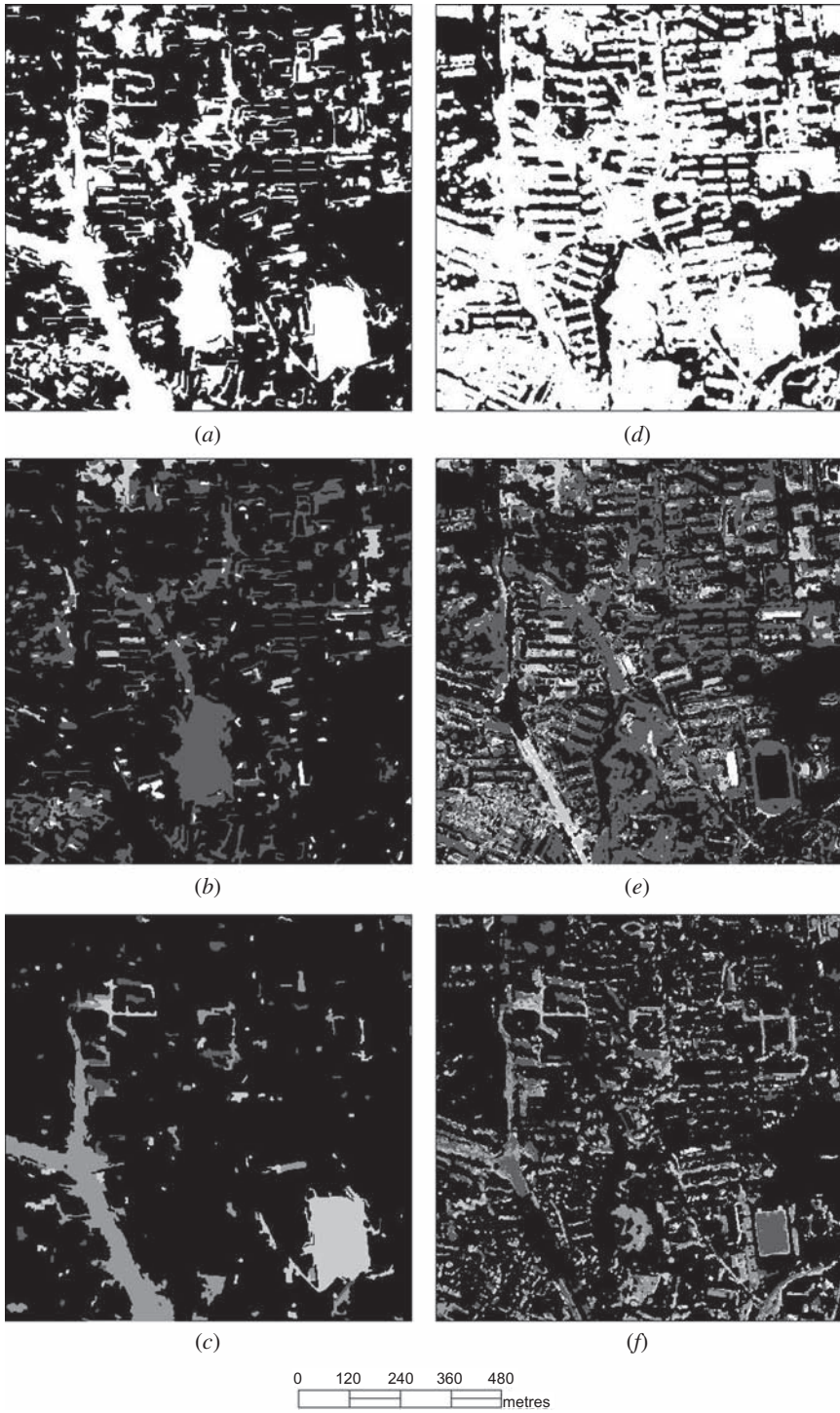


Figure 12. Comparison of the results of our method and the pixel-based CVA in site 2. (a) Binary change map of our method, (b) the first band of change direction map of our method, (c) the second band of change direction map of our method, (d) binary change map of the pixel-based CVA, (e) the first band of change direction map of the pixel-based CVA and (f) the second band of change direction map of the pixel-based CVA.

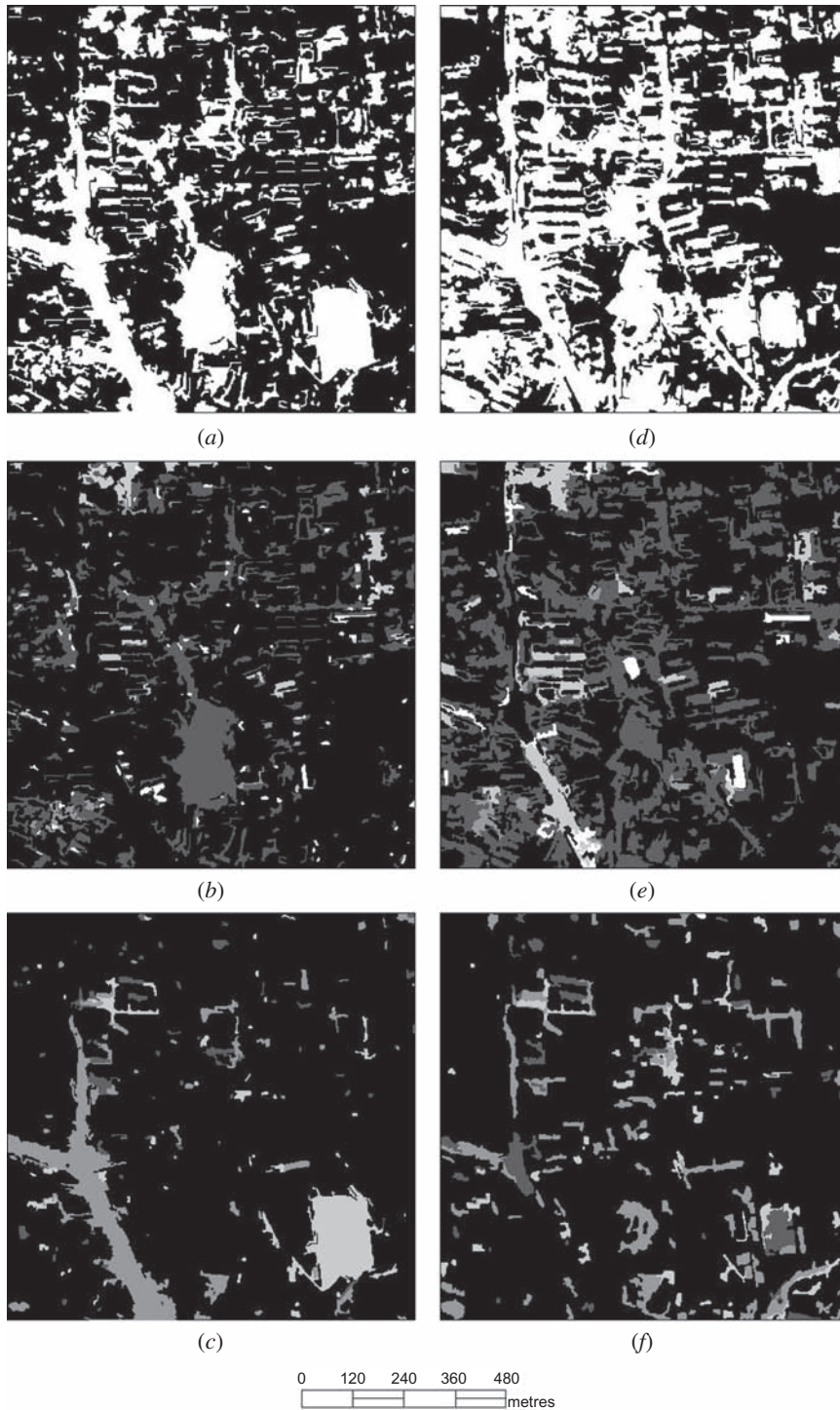


Figure 13. Comparison of the results of our method and the object-oriented CVA in Site 2. (a) Binary change map of our method, (b) the first band of change direction map of our method, (c) the second band of change direction map of our method, (d) binary change map of the object-oriented CVA, (e) the first band of change direction map of the object-oriented CVA and (f) the second band of change direction map of the object-oriented CVA.

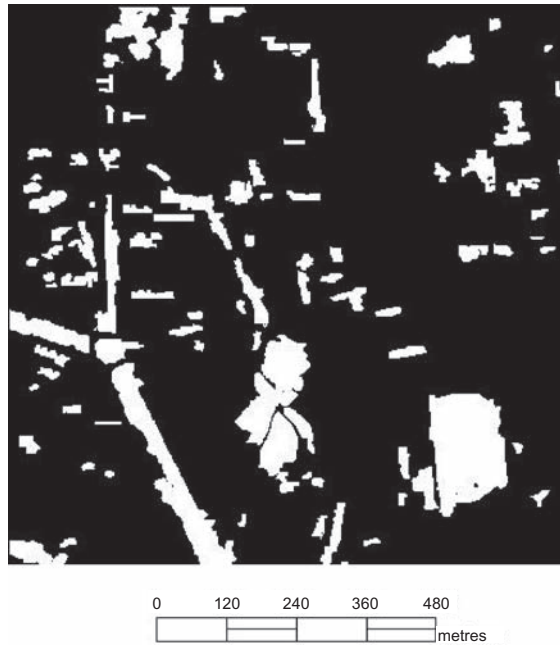


Figure 14. Reference map of changed area in site 2.

12 and a threshold of one (figure 13(d)–(f)). The integrity of the proposed method in large areas is obviously better than the object-oriented CVA.

Comparing the binary change map of our method to the reference one (figure 14), the proposed method could be proved to be reasonable. Nevertheless, there were some inevitable errors. The false alarms are primarily due to the relatively large objects on the edges of changed areas. The false alarms are also due to the illumination variance and shadow covering. On the other hand, the missed alarms primarily result from the relatively small objects in the change areas.

4. Discussion and conclusion

In this article, a new object-oriented method of change detection is proposed for high-resolution multispectral images. In the proposed method, after the segmentation of FNEA with a single scale, some small objects representing a same ground object were merged. During change detection with multi-scale object maps, each pair of objects were detected individually with the K–S test, according to the initial values of pixels in each object in this pair. Therefore, to detect the changed areas, full use could be made of spectral information in the initial images, while ignoring the redundant details included in the objects. By detecting object to object, it additionally considered the spatial features in the images.

The advantage of the object-oriented technique in processing high-resolution remote-sensing imagery is that changes in every object are detected instead of every pixel. It is effective in reducing the local spectral invariance and avoids the salt-pepper effect. On the other hand, being different from the object-oriented CVA, the proposed method uses the statistical probability of initial spectral values of pixels in every object,

instead of the mean values. This can avoid the information loss when just calculating the mean value. In our experimental results in the study areas, the overall errors of the proposed method were reduced by over 1000 pixels compared to the object-oriented CVA, which presents the superiority of our method.

The proposed method has proved to be an improvement on the current methods. However, it still has some shortcomings. It is affected by the robustness of the segmentation algorithm and the confusion method of multi-scale objects. In future, attempts will be made to consider other features together with the spectral information, such as texture and elevation.

Acknowledgements

This work was supported by Major State Basic Research Development Program (973 Program) under Grant 2009CB723905, the National Science Foundation of China (40930532, 41061130553), the Fundamental Research Funds for the Central Universities (3101016), and the LIESMARS Special Research Funding from Dr. Xin Huang. The authors would like to thank the editor and referees for their helpful suggestions which significantly improved the manuscript.

References

- BAATZ, M. and SCHAPE, A., 2000, Multiresolution segmentation – an optimization approach for high quality multi-scale image segmentation. In *Angewandte Geogr. Informationsverarbeitung XII*, J. Strobl and T. Blaschke (Eds.), pp. 12–23 (Heidelberg: Wichmann).
- BOVOLO, F., 2009, A multilevel parcel-based approach to change detection in very high resolution multitemporal images. *IEEE Geoscience and Remote Sensing Letters*, **6**, pp. 33–37.
- BRUZZONE, L. and PRIETO, D.F., 2000, Automatic analysis of the difference image for unsupervised change detection. *IEEE Transactions on Geoscience and Remote Sensing*, **38**, pp. 1171–1182.
- HUANG, X., ZHANG, L.P. and LI, P.X., 2007, Classification and extraction of spatial features in urban areas using high-resolution multispectral imagery. *IEEE Geoscience and Remote Sensing Letters*, **4**, pp. 260–264.
- HUANG, X., ZHANG, L.P. and WANG, L., 2009, Evaluation of morphological texture features for mangrove forest mapping and species discrimination using multispectral IKONOS imagery. *IEEE Geoscience and Remote Sensing Letters*, **6**, pp. 393–397.
- JOHNSON, R.D. and KASISCHKE, E.S., 1998, Change vector analysis: a technique for the multispectral monitoring of land cover and condition. *International Journal of Remote Sensing*, **19**, pp. 411–426.
- OLSON, G.A., CHERIYADAT, A., MALI, P. and O'HARA, C.G., 2004, Detecting and managing change in spatial data-land use and infrastructure change analysis and detection. *IEEE International Geoscience and Remote Sensing Symposium (IGARSS 2004)*, 1–3 January 2004, Anchorage, AL, pp. 729–734.
- PEARSON, E.S. and HARTLEY, H.O., 1972, *Biometrika Tables for Statisticians* (Cambridge: Cambridge University Press), Vol. 2, Table 55.
- SIEGEL, S. and CASTELLAN JR, N.J., 1988, *Nonparametric Statistics for the Behavioral Sciences*, pp. 127–135 (New York: McGraw-Hill).
- SINGH, A., 1989, Digital change detection techniques using remotely sensed data. *International Journal of Remote Sensing*, **10**, pp. 989–1003.
- SMIRNOV, N., 1948, Tables for estimating the goodness of fit of empirical distributions. *Annals of Mathematical Statistics*, **19**, pp. 280–281.

- WALTER, V., 2003, Object-based classification of remote sensing data for change detection. *ISPRS Journal of Photogrammetry and Remote Sensing*, **58**, pp. 225–238.
- WIKIPEDIA, 2009, Available online at: http://en.wikipedia.org/wiki/Main_Page (accessed 10 January 2010).
- ZHANG, L.P., HUANG, X., HUANG, B. and LI, P.X., 2006, A pixel shape index coupled with spectral information for classification of high spatial resolution remotely sensed imagery. *IEEE Transactions on Geoscience and Remote Sensing*, **44**, pp. 2950–2961.